Inorg. Chem. **2002**, *41*, 582–589

Coordination-Position Isomeric $M^{II}Cu^{II}$ and $Cu^{II}M^{II}$ (M = Co, Ni, Zn) Complexes Derived from Macrocyclic Compartmental Ligands

Masami Yonemura, Keisuke Arimura, Koji Inoue, Naoki Usuki, Masaaki Ohba, and Hisashi Ōkawa*

Department of Chemistry, Faculty of Science, Kyushu University, Hakozaki, Higashiku 6-10-1, Fukuoka 812-8581, Japan

Received May 14, 2001

The dinucleating macrocyclic ligands $(L^{2;2})^{2-}$ and $(L^{2;3})^{2-}$, comprised of two 2-[(*N*-methylamino)methyl]-6-(iminomethyl)-4-bromophenolate entities combined by the $-(CH_2)_2-$ chain between the two aminic nitrogen atoms and by the $-(CH_2)_2-$ or $-(CH_2)_3-$ chain between the two iminic nitrogen atoms, have afforded the following $M^{II}Cu^{II}$ complexes: $[CoCu(L^{2;2})](ClO_4)_2$·MeCN (**1A**), $[NiCu(L^{2;2})](ClO_4)_2$ (**2A**), $[ZnCu(L^{2;2})](ClO_4)_2$·0.5MeCN·EtOH (**3A**), $[CoCu(L^{2;3})(MeCN)(2\text{-PrOH})](ClO_4)_2$ (**4A**), $[NiCu(L^{2;3})](ClO_4)_2$ (**5A**), and $[ZnCu(L^{2;3})](ClO_4)_2$·1.5DMF (**6A**). $[CoCu(L^{2;2})(MeCN)_3](ClO_4)_2$ (**1A′**) crystallizes in the monoclinic space group $P2_1/n$, $a = 11.691(2)$ Å, $b = 18.572(3)$ Å, $c = 17.058(3)$ Å, $\beta = 91.18(2)°$, $V = 3703(1)$ Å^3, and $Z = 4$. $[NiCu(L^{2;2})(DMF)_2](ClO_4)_2$ (**2A′**) crystallizes in the triclinic space group $P\bar{1}$, $a = 11.260(2)$ Å, $b = 16.359(6)$ Å, $c = 10.853(4)$ Å, $\alpha = 96.98(3)°$, $\beta = 91.18(2)°$, $\gamma = 75.20(2)°$, $V = 1917(1)$ Å^3, and $Z = 2$. **4A** crystallizes in the monoclinic space group $P2_1/c$, $a = 15.064(8)$ Å, $b = 11.434(5)$ Å, $c = 21.352(5)$ Å, $\beta = 95.83(2)°$, $V = 3659(2)$ Å^3, and $Z = 4$. The X-ray crystallographic results demonstrate the M^{II} to reside in the $N(amine)_2O_2$ site and the Cu^{II} in the $N(imine)_2O_2$ site. The complexes **1**–**6** are regarded to be isomeric with $[CuCo(L^{2;2})](ClO_4)_2$·DMF (**1B**), $[CuNi(L^{2;2})](ClO_4)_2$·DMF·MeOH (**2B**), $[CuZn(L^{2;2})](ClO_4)_2$·H_2O (**3B**)), $[CuCo(L^{2;3})](ClO_4)_2$·$2H_2O$ (**4B**), $[CuNi(L^{2;3})](ClO_4)_2$ (**5B**), and $[CuZn(L^{2;3})](ClO_4)_2$·H_2O (**6B**) reported previously, when we ignore exogenous donating and solvating molecules. The isomeric $M^{II}Cu^{II}$ and $Cu^{II}M^{II}$ complexes are differentiated by X-ray structural, magnetic, visible spectroscopic, and electrochemical studies. The two isomeric forms are significantly stabilized by the "macrocyclic effect" of the ligands, but **1A** is converted into **1B** on an electrode, and **2A** is converted into **2B** at elevated temperature.

Introduction

Phenol-based macrocyclic ligands having two dissimilar metal-binding sites sharing two phenolic oxygen atoms have been used for the study of di-μ-phenolato heterodinuclear metal complexes.[1−5] The macrocyclic ligands $(L^{m;n})^{2-}$ (Chart 1)[2] show a site specificity of metal ions in producing $Cu^{II}M^{II}$ or $M^{II}Cu^{II}$ complexes depending upon the synthetic procedure and the nature of the counteranion used (the "M_aM_b complex" and formulation $[M_aM_b(L^{m;n})]^{2+}$ mean the M_a to reside in the aminic site and M_b in the iminic site). The dinuclear $M^{II}Cu^{II}$ chloride complexes $[MCu(L^{m;n})Cl_2]$ ($(L^{m;n})^{2-}$ =

Chart 1. Chemical Structure of $(L^{m;n})^{2-}$

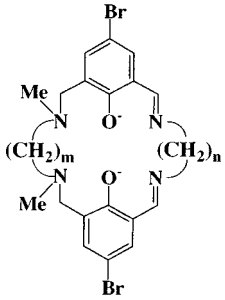

* Author to whom correspondence should be addressed. E-mail: okawascc@mbox.nc.kyushu-u.ac.jp.

(1) Ōkawa, H.; Furutachi, H.; Fenton, D. E. *Coord. Chem. Rev.* **1998**, *174*, 51.
(2) (a) Yonemura, M.; Matsumura, Y.; Ohba, M.; Ōkawa, H.; Fenton, D. E. *Chem. Lett.* **1996**, 601. (b) Yonemura, M.; Matsumura, Y.; Furutachi, H.; Ohba, M.; Ōkawa, H.; Fenton, D. E. *Inorg. Chem.* **1997**, *36*, 2711. (c) Yonemura, M.; Ohba, M.; Takahashi, K.; Ōkawa, H.; Fenton, D. E. *Inorg. Chim. Acta* **1998**, *283*, 72. (d) Yonemura, M.; Nakamura, Y.; Usuki, N.; Ōkawa, H. *Proc. Ind. Acad. Sci. (Chem. Ser.)* **2000**, *112*, 291. (e) Yonemura, M.; Usuki, N.; Nakamura, Y.; _kawa, H. *J. Chem. Soc., Dalton Trans.* **2000**, 3624.
(3) Fraser, C.; Johnston, L.; Rheingold, A. L.; Haggerty, B. S.; Williams, G. K.; Whelan, J.; Bosnich, B. *Inorg. Chem.* **1992**, *31*, 1835. McCollum, D. G.; Yap, G. P. A.; Rheingold, A. L.; Bosnich, B. *J. Am. Chem. Soc.* **1996**, *118*, 1365 and references therein.
(4) Karunakaran, S.; Kandaswamy, M. *J. Chem. Soc., Dalton Trans.* **1994**, 1595.
(5) Rybak-akimova, E. V.; Alcock, N. W.; Busch, D. H. *Inorg. Chem.* **1998**, *37*, 1563.

10.1021/ic010499d CCC: $22.00
Published on Web 01/12/2002

Scheme 1. Synthetic Schemes for $M^{II}Cu^{II}$ Chloride Complexes (I), $Cu^{II}M^{II}$ Perchlorate Complexes (II), and $M^{II}Cu^{II}$ Perchlorate Complexes (III)

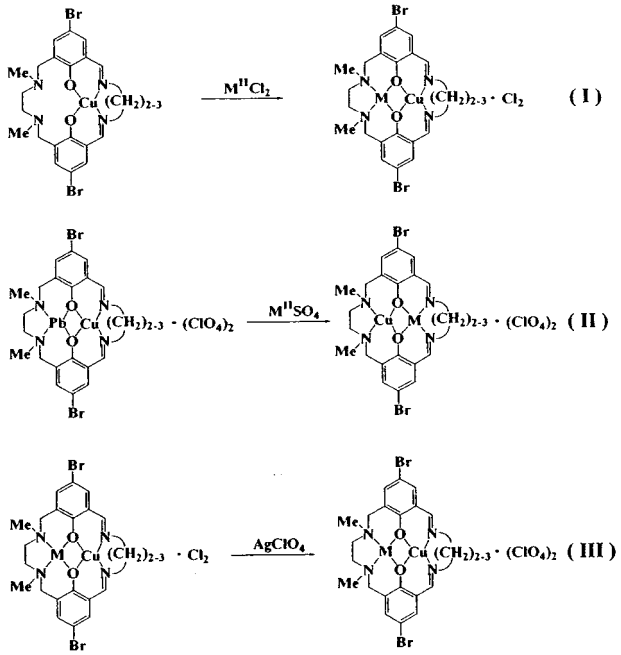

$(L^{2;2})^{2-}$, $(L^{2;3})^{2-}$, $(L^{2;4})^{2-}$; M = Mn^{II}, Co^{II}, Ni^{II}, Zn^{II}) have been derived from the mononuclear Cu^{II} precursors $[Cu(L^{m;n})]$ by the reaction with M^{II} chloride salts (Scheme 1, I).[2c] On the other hand, the transmetalation of the Pb^{II} in the $Pb^{II}Cu^{II}$ precursors $[PbCu(L^{m;n})](ClO_4)_2$ ($(L^{m;n})^{2-}$ = $(L^{2;2})^{2-}$ and $(L^{2;3})^{2-}$) for a M^{II} ion afforded the $Cu^{II}M^{II}$ perchlorate complexes $[CuM(L^{m;n})](ClO_4)_2$ (M = Co^{II}, Ni^{II}, Zn^{II}) (Scheme 1, II).[2b] In this reaction the Cu^{II} migrates from the iminic site to the aminic site to accommodate the M^{II} in the iminic site. The Cu migration in the transmetalation reaction is kinetically controlled by a geometrical characteristic of the macrocyclic ligands.[2d,e]

In this work we aim to provide coordination-position isomeric $M^{II}Cu^{II}$ and $Cu^{II}M^{II}$ complexes using $(L^{2;2})^{2-}$ and $(L^{2;3})^{2-}$. The following $M^{II}Cu^{II}$ perchlorate complexes have been obtained by the treatment of the $M^{II}Cu^{II}$ chloride complexes with $AgClO_4$: $[CoCu(L^{2;2})](ClO_4)_2 \cdot CH_3CN$ (**1A**), $[NiCu(L^{2;2})](ClO_4)_2$ (**2A**), $[ZnCu(L^{2;2})](ClO_4)_2 \cdot 0.5CH_3CN \cdot$ EtOH (**3A**), $[CoCu(L^{2;3})(CH_3CN)(2\text{-PrOH})](ClO_4)_2$ (**4A**), $[NiCu(L^{2;3})](ClO_4)_2$ (**5A**), and $[ZnCu(L^{2;3})](ClO_4)_2 \cdot 1.5DMF$ (**6A**)) (see Scheme 1, III). They are regarded as coordination-position isomers with the $Cu^{II}M^{II}$ perchlorate complexes $[CuM(L^{2;2})](ClO_4)_2$ (M = Co (**1B**), Ni (**2B**), Zn (**3B**)) and $[CuM(L^{2;3})](ClO_4)_2$ (M = Co (**4B**), Ni (**5B**), Zn (**6B**)), prepared by method II previously,[2b] when we ignore the exogenous donating and solvating molecules. Crystal structures of $[CoCu(L^{2;2})(CH_3CN)_3](ClO_4)_2$ (**1A′**), $[NiCu(L^{2;2})(DMF)_2](ClO_4)_2$ (**2A′**), and **4A** have been determined to see the site specificity of metal ions, and the physicochemical properties of **1A**−**6A** have been studied in comparison with those of isomeric **1B**−**6B**. The two isomeric forms, **1A**−**6A** and **1B**−**6B**, are significantly stabilized by the "macrocyclic effect" of the ligands, although **1A** was converted into **1B** on an electrode and **2A** was converted into **2B** at elevated temperature.

Experimental Section

Physical Measurements. Elemental analyses of C, H, and N were obtained at The Service Center of Elemental Analysis of Kyushu University. Metal analyses were made on a Shimadzu AA-680 atomic absorption/flame emission spectrophotometer. Infrared spectra were recorded on a Perkin-Elmer BX FT-IR system using KBr disks. Fast atom bombardment (FAB) mass spectra were recorded on a JMS-SX/SX102A Tundem mass spectrometer using *m*-nitrobenzyl alcohol as the matrix. Electronic absorption spectra in dimethyl sulfoxide (DMSO) and reflectance spectra on a powdered sample were recorded on a Shimadzu UV-3100PC spectrophotometer. Molar conductances were measured in DMSO with a DKK AOL-10 conductivity meter. Magnetic susceptibilities of powdered samples were measured on a Quantum Design MPMS XL SQUID susceptometer. The apparatus was calibrated with $[Ni(en)_3]S_2O_3$.[6] Diamagnetic corrections for the constituting atoms were made using Pascal's constants.[7] Cyclic voltammograms were measured using a BAS CV-50W electrochemical analyzer in DMSO solution containing tetra(*n*-butyl)ammonium perchlorate (TBAP) as the supporting electrolyte *(Caution! TBAP is explosive and should be handled with great care.)* A three-electrode cell was used which was equipped with a glassy carbon working electrode, a platinum coil as the counter electrode, and a Ag/Ag^+ (TBAP/acetonitrile) electrode as the reference.

Preparation. The $M^{II}Cu^{II}$ chloride complexes, $[MCu(L)Cl_2]$ (L = $(L^{2;2})^{2-}$, $(L^{2;3})^{2-}$; M = Co, Ni, Zn), were prepared by the literature method.[2c] Other chemicals were of reagent grade and used as purchased.

$M^{II}Cu^{II}$ Perchlorate Complexes. A solution of $AgClO_4$ (1.4 mmol) in ethanol (10 cm^3) was added to a suspension of each $[MCu(L^{m;n})Cl_2]$ (0.7 mmol) in acetonitrile (20 cm^3), and the mixture was stirred overnight at room temperature. The resulting AgCl was removed by filtration, and the filtrate was diffused with 2-propanol to obtain the respective $M^{II}Cu^{II}$ perchlorate complex. It was separated by filtration, washed with diethyl ether, and dried in air.

$[CoCu(L^{2;2})](ClO_4)_2 \cdot CH_3CN$ (1A). Red-brown crystals. Yield: 16%. Anal. Calcd for $C_{24}H_{27}Br_2Cl_2CoCuN_5O_{10}$: C, 32.08; H, 3.03; N, 7.79; Co, 6.56; Cu, 7.07. Found: C, 32.25; H, 3.22; N, 8.02; Co, 6.39; Cu, 6.96. Selected IR (ν/cm^{-1}) using KBr: 1632, 1441, 1288, 1085, 620. μ_{eff} per CoCu: 4.52 μ_B at 290 K. UV−vis [λ_{max}/nm (ϵ/M^{-1} cm^{-1})]: 350 (7710), 540 (180) in DMSO. Molar conductance [Λ_M/S cm^2 mol^{-1}]: 63 in DMSO.

Single crystals of $[CoCu(L^{2;2})(CH_3CN)_3](ClO_4)_2$ (**1A′**) suitable for X-ray crystallography were grown from the filtrate.

$[NiCu(L^{2;2})](ClO_4)_2$ (2A). Brown microcrystals. Yield: 42%. Anal. Calcd for $C_{24}H_{27}Br_2Cl_2CuN_5NiO_{10}$: C, 32.08; H, 3.03; N, 7.80; Cu, 7.07; Ni, 6.53. Found: C, 32.02; H, 3.07; N, 7.62; Cu, 7.76; Ni, 5.71. Selected IR (ν/cm^{-1}) using KBr: 1628, 1442, 1275, 1096, 622. μ_{eff} per NiCu: 3.26 μ_B at 290 K. UV−vis [λ_{max}/nm (ϵ/M^{-1} cm^{-1})]: 355 (6180), 570 (145) in DMSO. Molar conductance [Λ_M/S cm^2 mol^{-1}]: 30 in DMSO.

Single crystals of $[NiCu(L^{2;2})(DMF)_2](ClO_4)_2$ (**2A′**) suitable for X-ray crystallographic studies were obtained when a DMF solution of **2A** was diffused with 2-propanol.

$[ZnCu(L^{2;2})](ClO_4)_2 \cdot 0.5CH_3CN \cdot EtOH$ (3A). Purple microcrystals. Yield: 23%. Anal. Calcd for $C_{25}H_{30.5}Br_2Cl_2CuN_{4.5}O_{11}Zn$: C, 32.30; H, 3.31; N, 6.78; Cu, 6.84; Zn, 7.03. Found: C, 32.53; H, 3.04; N, 6.78; Cu, 7.31; Zn, 7.37. Selected IR (ν/cm^{-1}) using KBr: 1626, 1445, 1290, 1108, 621. μ_{eff} per ZnCu: 1.87 μB at 290

(6) Curtis, N. F. *J. Chem. Soc.* **1961**, 3147.
(7) Landolt-Börnstein. Neue Series II/11; Springer-Verlag: Berlin, 1981.

Table 1. Crystallograhic Data of **1A′**, **2A′**, and **4A**

	1A′	2A′	4A
empirical formula	$C_{28}H_{33}Br_2Cl_2CoCuN_7O_{10}$	$C_{28}H_{38}Br_2Cl_2CuN_4NiO_{12}$	$C_{28}H_{37}Br_2Cl_2CoCuN_4O_{11}$
fw	980.80	1003.60	972.82
cryst syst	monoclinic	triclinic	monoclinic
space group	$P2_1/n$ (no. 14)	$P\bar{1}$ (no. 2)	$P2_1/c$ (no. 14)
a/Å	11.691(2)	11.260(2)	15.064(8)
b/Å	18.572(3)	16.359(6)	11.434(5)
c/Å	17.058(3)	10.853(4)	21.354(5)
α/deg	96.98(3)		
β/deg	91.18(2)	94.36(2)	95.83(3)
γ/deg	75.20(2)		
V/Å^3	3703.0(10)	1916.5(9)	3659(2)
Z	4	2	4
D_{calcd}/ g cm^{-3}	1.759	1.739	1.766
μ(Mo Kα)/cm^{-1}	33.93	33.41	34.33
no. of reflns ($I > 3.00\sigma(I)$)	3514	6379	4224
F(000)	1960	1010	1952
R[a]	0.078	0.048	0.081
R$_w$[b]	0.073	0.035	0.086

[a] $R = \sum||F_o| - |F_c||/\sum|F_o|$. [b] $R_w = [\sum w(|F_o| - |F_c|)^2/\sum w|F_o|^2]^{1/2}$ with $w = 1/\sigma(|F_o|)^2$.

K. UV−vis (λ_{max}/nm (ϵ/M^{-1} cm^{-1})]: 351 (7770), 553 (190) in DMSO. Molar conductance [Λ_M/S cm^2 mol^{-1}]: 47 in DMSO.

[CoCu(L$^{2;3}$)(CH$_3$CN)(2-PrOH)](ClO$_4$)$_2$ (4A). Brown crystals. Yield: 44%. Anal. Calcd for $C_{28}H_{37}Br_2Cl_2CoCuN_5O_{11}$: C, 34.57; H, 3.83; N, 7.20; Cu, 6.53; Co, 6.06. Found: C, 34.67; H, 3.83; N, 7.36; Cu, 6.68; Co, 6.25. Selected IR (ν/cm^{-1}) using KBr: 1620, 1454, 1299, 1103, 624. μ_{eff} per CoCu: 4.36 μ_B at 290 K. UV−vis [λ_{max}/nm (ϵ/M^{-1} cm^{-1})]: 352 (9170), 640 (106) in DMSO. Molar conductance [Λ_M/S cm^2 mol^{-1}]: 64 in DMSO.

[NiCu(L$^{2;3}$)](ClO$_4$)$_2$ (5A). Green microcrystals. Yield: 35%. Anal. Calcd for $C_{23}H_{26}Br_2Cl_2CuN_4NiO_{10}$: C, 31.70; H, 3.01; N, 18.34; Cu, 7.29; Ni, 6.74. Found: C, 31.73; H, 2.93; N, 6.55; Cu, 7.45; Ni, 5.38. Selected IR (ν/cm^{-1}) using KBr: 1624, 1456, 1300, 1101, 622. μ_{eff} per NiCu: 3.37 μ_B at 290 K. UV−vis [λ_{max}/nm (ϵ/M^{-1} cm^{-1})]: 353 (9650), 634 (111) in DMSO. Molar conductance [Λ_M/S cm^2 mol^{-1}]: 59 in DMSO.

[ZnCu(L$^{2;3}$)](ClO$_4$)$_2$·1.5DMF (6A). Green microcrystalline powder. Yield: 29%. Anal. Calcd for $C_{27.5}H_{36.5}Br_2Cl_2CuN_{5.5}O_{11.5}Zn$: C, 33.44; H, 3.72; N, 7.80; Cu, 6.43; Zn, 6.62. Found: C, 33.14; H, 4.00; N, 7.55; Cu, 6.11; Zn, 6.59. Selected IR (ν/cm^{-1}) using KBr: 1659, 1620, 1452, 1303, 1095, 624. μ_{eff} per ZnCu: 1.88 μ_B at 290 K. UV−vis [λ_{max}/nm (ϵ/M^{-1} cm^{-1})]: 350 (8320), 643 (87) in DMSO. Molar conductance [Λ_M/S cm^2 mol^{-1}]: 54 in DMSO.

Cu^{II}M^{II} Perchlorate Complexes (M = Co, Ni, Zn). The M^{II}-Cu^{II} perchlorate complexes [CuCo(L$^{2;2}$)](ClO$_4$)$_2$·DMF (**1B**), [CuNi(L$^{2;2}$)](ClO$_4$)$_2$·DMF·MeOH (**2B**), [CuZn(L$^{2;2}$)](ClO$_4$)$_2$·H$_2$O (**3B**)), [CuCo(L$^{2;3}$)](ClO$_4$)$_2$·2H$_2$O (**4B**), [CuNi(L$^{2;3}$)](ClO$_4$)$_2$ (**5B**), and [CuZn(L$^{2;3}$)](ClO$_4$)$_2$·H$_2$O (**6B**) were prepared by the methods described previously.[2b,e]

X-ray Crystallography. Each single crystal of **1A′**, **2A′**, and **4A** was sealed in a glass tube and used for measurements on a Rigaku AFC7R diffractometer with graphite-monochromated Mo Kα radiation (λ = 0.71069 Å) and a 12 kW rotating anode generator. The cell constant and an orientation matrix for the data collection were obtained from 25 reflections, and the $\omega-2\theta$ scan mode was used for the intensity corrections at 23 ± 1 °C. The octant measured was $+h$, $+k$, $\pm l$ for all the complexes. Pertinent crystallographic parameters are summarized in Table 1.

Three standards were monitored every 150 measurements. Over the course of data collection, the standards decreased by 5.2% for **1A′**, 1.3% for **2A′**, and 0.1% for **4A**. A linear correction factor was applied to the data to account for the phenomena. Intensity data were corrected for Lorentz and polarization effects.

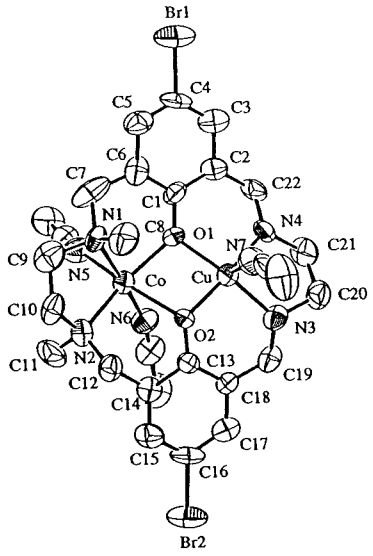

Figure 1. An ORTEP view of **1A′** with the atom numbering system.

The structures were solved by a direct method and expanded using Fourier techniques. The non-hydrogen atoms were refined anisotropically. All calculations were carried out on an IRIS Indy O2 computer using the TEXSAN crystallographic software package.[8]

Results and Discussion

Crystal Structures. 1. [CoCu(L$^{2;2}$)(CH$_3$CN)$_3$](ClO$_4$)$_2$ (1A′). An ORTEP[9] view of the cationic part is shown in Figure 1 together with the numbering scheme. Selected bond distances and angles are given in Table 2.

X-ray crystallography clearly demonstrates that the Co resides in the aminic site and the Cu in the iminic site as found for the parent complex [CoCu(L$^{2;2}$)Cl$_2$].[2e] The Co···Cu intermetallic separation bridged by the two phenolic oxygen atoms is 3.025(2) Å. The Co−O1−Cu and Co−O2−Cu angles are 101.0(4)° and 94.5(3)°, respectively.

(8) TEXSAN, Molecular Structure Analysis Package, Molecular Structure Corp., Houston, TX, 1985, 1992.
(9) Johnson, C. K. Report 3794; Oak Ridge National Laboratory: Oak Ridge, TN, 1976.

Table 2. Selected Bond Distances and Angles for **1A′**

	Bond Distances (Å)		
Co−O(1)	1.997(9)	Cu−O(1)	1.923(8)
Co−O(2)	2.196(8)	Cu−O(2)	1.917(8)
Co−N(1)	2.148(10)	Cu−N(3)	1.92(1)
Co−N(2)	2.15(1)	Cu−N(4)	1.92(1)
Co−N(5)	2.12(1)	Cu−N(7)	2.45(1)
Co−N(6)	2.14(1)	Co···Cu	3.025(2)
	Bond Angles (deg)		
Co−O(1)−Cu	101.0(4)	N(2)−Co−N(5)	105.6(5)
Co−O(2)−Cu	94.5(3)	N(2)−Co−N(6)	98.6(4)
O(1)−Co−O(2)	75.3(3)	N(5)−Co−N(6)	83.2(4)
O(1)−Co−N(1)	81.8(4)	O(1)−Cu−O(2)	83.8(3)
O(1)−Co−N(2)	151.5(4)	O(1)−Cu−N(3)	160.6(4)
O(1)−Co−N(5)	98.3(4)	O(1)−Cu−N(4)	90.5(4)
O(1)−Co−N(6)	99.4(4)	O(1)−Cu−N(7)	103.4(4)
O(2)−Co−N(1)	108.4(3)	O(2)−Cu−N(3)	95.9(5)
O(2)−Co−N(2)	86.6(4)	O(2)−Cu−N(4)	169.4(4)
O(2)−Co−N(5)	160.0(4)	O(2)−Cu−N(7)	90.3(4)
O(2)−Co−N(6)	79.3(4)	N(3)−Cu−N(4)	86.4(5)
N(1)−Co−N(2)	83.4(4)	N(3)−Cu−N(7)	96.0(5)
N(1)−Co−N(5)	89.1(4)	N(4)−Cu−N(7)	99.7(5)
N(1)−Co−N(6)	172.3(4)		

The geometry about the Cu is square-pyramidal with an acetonitrile nitrogen (N7) at the apex; the discriminating parameter τ[10] between a square pyramid ($\tau = 0$) and a trigonal bipyramid ($\tau = 1$) is 0.147. The equatorial Cu-to-ligand bond distances fall in the range of 1.917(8)−1.923(8) Å. The axial Cu−N7 bond is elongated (2.45(1) Å) owing to the Jahn−Teller effect for the d^9 electronic configuration of Cu^{II}. The displacement of the Cu from the basal least-squares plane toward N7 is 0.242 Å. The O1−N1−N2−O2 part of the aminic site adopts a nonplanar chelating mode, providing a cis-β-octahedral geometry about the Co together with two acetonitrile nitrogens (N5 and N6) in cis positions. The Co-to-donor bond distances range from 1.997(9) to 2.196(8) Å. The asymmetric nitrogen atoms N1 and N2 have the same *S* configuration. The two methyl groups attached to N1 and N2 are situated trans with respect to the en−Co^{II} chelate ring.

2. $[NiCu(L^{2,2})(DMF)_2](ClO_4)_2$ (2A′). An ORTEP view of the cationic part is shown in Figure 2 together with the numbering scheme. Selected bond distances and angles are given in Table 3.

The cation has a discrete dinuclear core with the Ni^{II} in the aminic site and the Cu^{II} in the iminic site. The Ni···Cu intermetallic separation is 2.959(1) Å. The Cu has a planar geometry with Cu-to-ligand bond distances of 1.905(4)−1.925(3) Å. The displacement of the Cu from the basal N_2O_2 least-squares plane is small (0.147 Å). The Ni in the aminic site has a cis-β-octahedral configuration along with two DMF oxygen atoms (O3 and O4) in cis positions. The Ni-to-donor bond distances range from 2.045(3) to 2.177(3) Å. The asymmetric nitrogen atoms N1 and N2 have the same *S* configuration. The two methyl groups attached to N1 and N2 are situated trans with respect to the Ni−en chelate ring.

3. $[CoCu(L^{2,3})(CH_3CN)(2\text{-}PrOH)](ClO_4)_2$ (4A). An ORTEP view of the cationic part is shown in Figure 3 together with the numbering scheme. Selected bond distances and angles are given in Table 4.

(10) Johnson, C. K. Report 3794; Oak Ridge National Laboratory: Oak Ridge, TN, 1965.

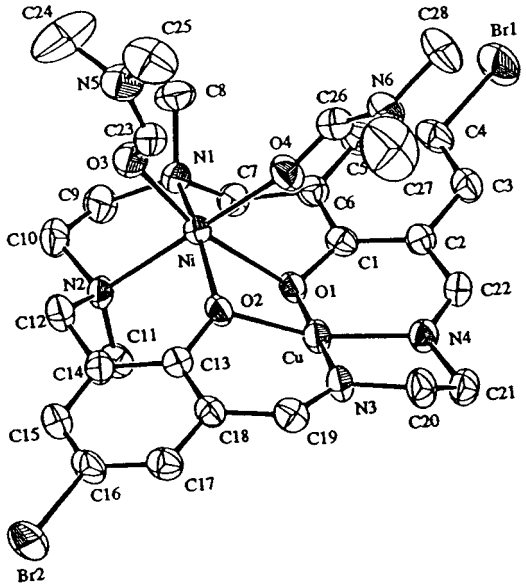

Figure 2. An ORTEP view of **2A′** with the atom numbering system.

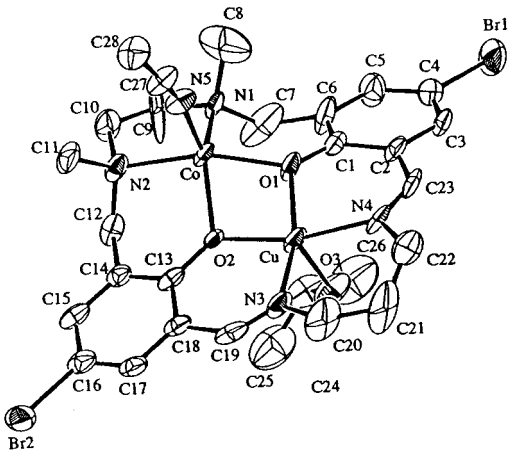

Figure 3. An ORTEP view of **4A** with the atom numbering system.

Table 3. Selected Bond Distances and Angles for **2A′**

	Bond Distances (Å)		
Ni−O(1)	2.177(3)	Cu−O(1)	1.925(3)
Ni−O(2)	2.045(3)	Cu−O(2)	1.907(3)
Ni−O(3)	2.025(3)	Cu−N(3)	1.921(4)
Ni−O(4)	2.120(3)	Cu−N(4)	1.905(4)
Ni−N(1)	2.107(4)	Ni···Cu	2.9594(9)
Ni−N(2)	2.099(4)		
	Bond Angles (deg)		
Ni−O(1)−Cu	92.1(1)	O(3)−Ni−N(1)	94.9(1)
Ni−O(2)−Cu	96.9(1)	O(3)−Ni−N(2)	88.0(1)
O(1)−Ni−O(2)	78.2(1)	O(4)−Ni−N(1)	107.7(1)
O(1)−Ni−O(3)	164.1(1)	O(4)−Ni−N(2)	166.2(1)
O(1)−Ni−O(4)	79.1(1)	N(1)−Ni−N(2)	84.7(1)
O(1)−Ni−N(1)	89.4(1)	O(1)−Cu−O(2)	88.0(1)
O(1)−Ni−N(2)	107.7(1)	O(1)−Cu−N(3)	178.9(1)
O(2)−Ni−O(3)	101.0(1)	O(1)−Cu−N(4)	95.3(1)
O(2)−Ni−O(4)	84.5(1)	O(2)−Cu−N(3)	90.9(1)
O(2)−Ni−N(1)	160.8(1)	O(2)−Cu−N(4)	162.5(2)
O(2)−Ni−N(2)	85.2(1)	N(3)−Cu−N(4)	85.6(2)
O(3)−Ni−O(4)	84.9(1)		

The result demonstrates a dinuclear core with the Co in the aminic site and the Cu in the iminic site. The Co···Cu intermetallic separation is 3.049(2) Å. The Co−O1−Cu and Co−O2−Cu angles are 101.0(3)° and 101.2(3)°, respectively.

Table 4. Selected Bond Distances and Angles for **4A**

	Bond Distances (Å)		
Co−O(1)	1.988(7)	Cu−O(1)	1.961(7)
Co−O(2)	1.997(7)	Cu−O(2)	1.949(7)
Co−N(1)	2.092(9)	Cu−O(3)	2.315(8)
Co−N(2)	2.108(10)	Cu−N(3)	1.963(10)
Co−N(5)	2.04(1)	Cu−N(4)	1.97(1)
		Co···Cu	3.049(2)
	Bond Angles (deg)		
Co−O(1)−Cu	101.0(3)	N(2)−Co−N(5)	94.4(4)
Co−O(2)−Cu	101.2(3)	O(1)−Cu−O(2)	77.3(3)
O(1)−Co−O(2)	75.6(3)	O(1)−Cu−O(3)	91.4(3)
O(1)−Co−N(1)	90.5(3)	O(1)−Cu−N(3)	164.6(4)
O(1)−Co−N(2)	158.5(4)	O(1)−Cu−N(4)	89.3(4)
O(1)−Co−N(5)	106.7(4)	O(2)−Cu−O(3)	95.6(3)
O(2)−Co−N(1)	136.9(4)	O(2)−Cu-N(3)	91.8(4)
O(2)−Co−N(2)	92.5(3)	O(2)−Cu−N(4)	165.8(3)
O(2)−Co−N(5)	113.2(3)	O(3)−Cu−N(3)	100.6(4)
N(1)−Co−N(2)	86.2(4)	O(3)−Cu−N(4)	89.4(4)
N(1)−Co−N(5)	109.9(4)	N(3)−Cu−N(4)	100.3(4)

The Cu has a square-pyramidal geometry with O3 of 2-PrOH at the apex. The equatorial Cu-to-donor bond distances fall in the range of 1.949(7)−1.97(1) Å. The axial Cu−O3 bond is elongated owing to the Jahn−Teller effect (2.315(8) Å). The displacement of the Cu from the basal N_2O_2 least-squares plane toward axial O3 is 0.143 Å.

The geometry about the Co is also square-pyramidal (τ = 0.36) with an acetonitrile nitrogen (N5) at the apex. The equatorial Co-to-ligand bond distances range from 1.988(7) to 2.108(10) Å. The axial Co−N5 bond distance is 2.04(1) Å. The deviation of the Co from the basal N_2O_2 least-squares plane toward N5 is 0.575 Å.

The ethylene lateral chain in the aminic site assumes a gauche conformation, and the trimethylene chain in the iminic site assumes a chair conformation. The asymmetric nitrogen atoms N1 and N2 have *S* and *R* configurations, respectively. The two methyl groups attached to N1 and N2 are situated cis to each other with respect to the mean molecular plane. The acetonitrile molecule bonded to the Co and the *N*-methyl groups are situated cis to each other. The 2-PrOH bound to the Cu and the acetonitrile bound to the Co are situated trans to each other. The basal least-squares plane of the aminic site and that of the iminic site are bent at the O1···O2 edge with a dihedral angle of 8.68°.

Physicochemical Properties. 1. Magnetic Properties. Complex **1A** (CoCu of $(L^{2;2})^{2-}$) has a magnetic moment of 4.52 μ_B at 290 K, and the moment decreases with decreasing temperature to 1.20 μ_B at 2.0 K (Figure 4). Evidently, the Co^{II} in the $N(amine)_2O_2$ site is of high spin, and the decrease in the magnetic moment suggests an antiferromagnetic interaction within each molecule. It is notable that the moment at 2.0 K (1.20 μ_B) is lower than the value expected for $S_T = 1$ arising from antiferromagnetic coupling between Cu^{II} (S = 1/2) and Co^{II} (S = 3/2). This fact implies the operation of a secondary magnetic effect at low temperature. Zero-field splitting of S_{Co} = 3/2 must be the secondary magnetic effect; the orbital contribution of $^4T_{1g}$ for O_h-symmetric Co^{II} can be neglected judged from a distorted geometry about the Co atom. Isomeric **1B** (CuCo) has a small magnetic moment of 3.22 μ_B at room temperature because the Co^{II} in the salen-like $N(imine)_2O_2$ site is of low spin.[2e]

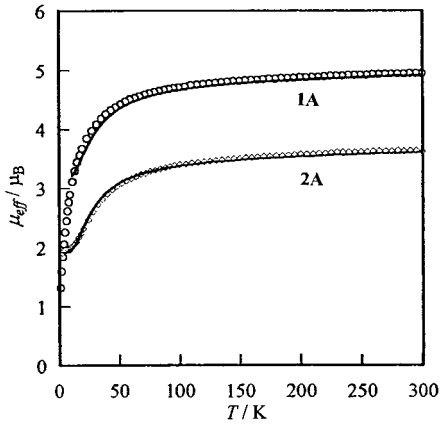

Figure 4. Temperature dependence of magnetic moments (per MCu) of **1A** and **2A**.

Complex **2A** (NiCu) has a subnormal magnetic moment of 3.26 μ_B at room temperature, and the moment decreases with decreasing temperature to 1.94 μ_B at 4 K (Figure 4). Isomeric **2B** (CuNi) has a room-temperature magnetic moment of 1.95 μ_B common for one unpaired electron because of the diamagnetic nature of the Ni^{II} in the iminic site.[2e]

On the basis of the isotropic Heisenberg model[11] ($H = -2\sum S_iS_j$) and by assuming no orbital degeneracy for the Co^{II}, the magnetic susceptibility expressions for the Co^{II} (S = 3/2)−Cu^{II} (S = 1/2) and Ni^{II} (S = 1)−Cu^{II} (S = 1/2) systems are given by eqs 1 and 2,

$$\chi_M = \{N\beta^2/kT\}[10g_2^2 + 2g_1^2\exp(-4J/kT)]/[5 + 3\exp(-4J/kT)] + N\alpha \quad (1)$$

$$\chi_M = \{N\beta^2/4kT\}[10g_{3/2}^2 + g_{1/2}^2\exp(-3J/kT)]/[2 + \exp(-3J/kT)] + N\alpha \quad (2)$$

respectively,[12] where N is Avogadro's number, β is the Bohr magneton, k is the Boltzmann constant, J is the exchange integral, T is the absolute temperature, and $N\alpha$ is the temperature-independent paramagnetism. The g_1 and g_2 in eq 1 are g factors associated with the total spin states S_T = 1 and 2, respectively, and are expressed using local g_{Co} and g_{Cu} factors as $g_1 = (5g_{Co} - g_{Cu})/4$ and $g_2 = (3g_{Co} + g_{Cu})/4$.[13,14] Similarly, the $g_{1/2}$ and $g_{3/2}$ in eq 2 are the g factors associated with the total spin states S_T = 1/2 and 3/2, respectively, and are expressed using local g_{Ni} and g_{Cu} factors as $g_{1/2} = (4g_{Ni} - g_{Cu})/3$ and $g_{3/2} = (2g_{Ni} + g_{Cu})/3$.

Magnetic simulations for **1A** using eq 1 gave a poor fit in the low-temperature region (<10 K) probably owing to the zero-field splitting of S_{Co} = 3/2, but a tolerable fit was obtained in the simulation in the region of 10−300 K using $J = -8.0$ cm^{-1}, $g_{Co} = 2.29$, $g_{Cu} = 2.13$, and $N\alpha = 300 \times 10^{-6}$ cm^3 mol^{-1} (Figure 4). The discrepancy factor defined

(11) Heisenberg, H. *Z. Phys*. **1926**, *38*, 411.
(12) (a) _kawa, H.; Nishida, Y.; Tanaka, M.; Kida, S. *Bull. Chem. Soc. Jpn*. **1977**, *50*, 127. (b) _kawa, H.; Nishio, J.; Ohba, M.; Tadokoro, M.; Matsumoto, N.; Koikawa, M.; Kida, S.; Fenton, D. E. *Inorg. Chem*. **1993**, *32*, 2949.
(13) Chao, C. C. *J. Magn. Reson*. **1973**, *10*, 1.
(14) Scaringe, R. P.; Hodgson, D. J.; Hatfield, W. E. *Mol. Phys*. **1978**, *35*, 701.

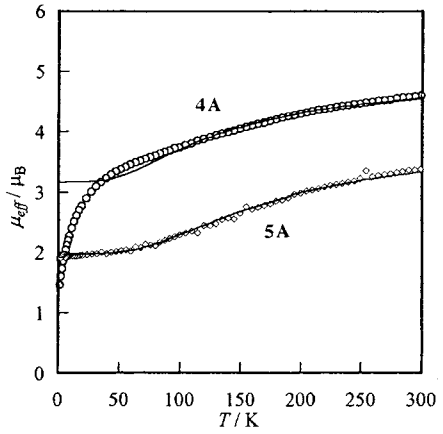

Figure 5. Temperature dependence of magnetic moments (per MCu) of **4A** and **5A**.

as $R(\chi) = [\sum(\chi_{obsd} - \chi_{calcd})^2/\sum(\chi_{obsd})^2]^{1/2}$ was 1.27×10^{-2}. The cryomagnetic property of **2A** can be well reproduced by eq 2 as indicated by the solid line in Figure 4, using $J = -12.0$ cm^{-1}, $g_{Cu} = 2.08$, $g_{Ni} = 2.18$, and $N\alpha = 280 \times 10^{-6}$ cm^3 mol^{-1}. The discrepancy factor in this simulation was 9.29×10^{-3}.

Complex **4A** (CoCu of $(L^{2;3})^{2-}$) has a subnormal magnetic moment of 4.36 μ_B at room temperature, and the moment decreases with decreasing temperature to 1.42 μ_B at 2.0 K (Figure 5). Again, the moment at 2.0 K is lower than the value expected for $S_T = 1$ arising from antiferromagnetic coupling between Cu^{II} ($S = 1/2$) and Co^{II} ($S = 3/2$). A difficulty arose in magnetic simulations of **4A** using eq 1; the solid line is drawn on the basis of eq 1 using $J = -38$ cm^{-1}, $g_{Co} = 2.29$, $g_{Cu} = 2.13$, and $N\alpha = 300 \times 10^{-6}$ cm^3 mol^{-1}. A large deviation between the empirical and theoretical curves in the temperature region lower that 100 K suggests a large zero-field splitting of $S_{Co} = 3/2$ in this complex. A similar difficulty in magnetic simulation was observed for isomeric **4B** previously.[2b]

Complex **5A** (NiCu) has a room-temperature magnetic moment of 3.37 μ_B, which decreases with decreasing temperature to a near plateau value of 1.98 μ_B at 50 K (Figure 5). Magnetic analyses for **5A** using eq 2 gave a tolerable fit using the parameters $J = -57$ cm^{-1}, $g_{Ni} = 2.17$, $g_{Cu} = 2.12$, $N\alpha = 350 \times 10^{-6}$ cm^3 mol^{-1}, and $\theta = 0$. A negatively larger exchange integral (-97.0 cm^{-1}) was recognized for isomeric **5B**.[2b]

Thus, **1A**, **2A**, and **5A** are differentiated by magnetic studies from **1B**, **2B**, and **5B**, respectively, although **4A** and **4B** could not be unambiguously differentiated. The $Zn^{II}Cu^{II}$ and $Cu^{II}Zn^{II}$ complexes **3A**, **3B**, **6A**, and **6B** have a magnetic moment common for one unpaired electron.

2. Electronic Spectra. Electronic spectra of the $M^{II}Cu^{II}$ complexes **1A**−**6A** have been studied in comparison with those of the $Cu^{II}M^{II}$ complexes **1B**−**6B** in DMSO. The numerical data are summarized in Table 5.

Complexes **1A** (CoCu), **2A** (NiCu), and **3A** (ZnCu) of $(L^{2;2})^{2-}$ show a distinct absorption band at 540−570 nm that is attributable to a superposed d−d band of the Cu^{II} in the iminic site.[15] Isomeric **1B** (CuCo), **2B** (CuNi), and **3B** (CuZn) have a d−d band maximum due to the Cu^{II} at longer wavelength (646−670 nm).[2e] In the case of **2B**, an additional absorption band is observed at 530 nm that is characteristic of low-spin Ni^{II}.[16,17] For **1A**, **2A**, and **1B** the d−d bands due to the M^{II} ion are not resolved because of a low extinction coefficient.

Complexes **4A** (CoCu), **5A** (NiCu), and **6A** (ZnCu) of $(L^{2;3})^{2-}$ show a d−d band maximum due to the Cu^{II} at 634−643 nm. In the spectra of **4B** (CuCo), **5B** (CuNi), and **6B** (CuZn) in DMSO, one or two d−d bands are observed: 571 and 612 nm for **4B**; 587 and 752 nm for **5B**; 639 nm for **6B**.[2b] Evidently, the spectrum of **4A** differs from that of **4B**, and the spectrum of **5A** differs from that of **5B**, though **6A** and **6B** cannot be differentiated by the visible spectra.

An intense absorption band is commonly seen near 350 nm for **1A**−**6A** and **1B**−**6B**. This band is assigned to the $\pi-\pi^*$ transition band associated with the azomethine group.[18,19]

3. Electrochemical Properties. Electrochemical properties of **1A**−**6A** were studied by means of cyclic voltammetry in DMSO. Electrochemical properties of **1B**−**3B** were also studied in this work. Electrochemical properties for **4B**−**6B** were reported previously.[2b] The numerical data are summarized in Table 6.

Complexes **1A** (CoCu), **2A** (NiCu), and **3A** (ZnCu) of $(L^{2;2})^{2-}$ show a quasi-reversible couple at -1.16 ± 0.02 V (vs Ag/Ag$^+$) attributable to the Cu^I/Cu^{II} process at the iminic site. No reduction occurred for the Co^{II} and Ni^{II} in the aminic site at the available potential. In the case of **3**, the cyclic voltammogram changed with the repeat of sweep, with the decrease of the couple at -1.18 V with concomitant appearance of a cathodic peak near -0.7 V and an anodic peak near -0.6 V. This fact means instability of the complex on the electrode. Isomeric **1B** (CuCo), **2B** (CuNi), and **3B** (CuZn) show a reversible or quasi-reversible couple at -0.55 ± 0.07 V that is attributed to the Cu^I/Cu^{II} process in the aminic site (see Figure 6). The reduction potentials for **1B**−**3B** are considerably high relative to those of **1A**−**3A**, indicating that the $\{CuN(amine)_2O_2\}$ chromophore is flexible enough to allow a distorted geometry preferred for Cu^I.[20] The CV of **1B** has an additional couple at -1.35 V attributable to the Co^I/Co^{II} process,[21] and the CV of **2B** has an additional couple at -1.76 V attributable to the Ni^I/Ni^{II} process[22] (see Figure 6).

Complexes **4A** (CoCu), **5A** (NiCu), and **6A** (ZnCu) of $(L^{2;3})^{2-}$ show a quasi-reversible Cu^I/Cu^{II} couple at -0.96 ± 0.04 V, whereas isomeric **4B** (CuCo), **5B** (CuNi), and **6B** (CuZn) show the Cu^I/Cu^{II} couple at -0.64 ± 0.05 V.[2b] Complex **4A** showed no other reduction wave, but **4B** showed another reversible couple at -1.64 V attributable to

(15) Ferguson, J. *J. Chem. Phys.* **1961**, *34*, 2206.
(16) Holm, R. H. *J. Am. Chem. Soc.* **1960**, *82*, 5632.
(17) Hoyt, W. C.; Everett, G. W., Jr. *Inorg. Chem.* **1969**, *8*, 2013.
(18) Bosnich, B. *J. Am. Chem. Soc.* **1968**, *90*, 627.
(19) Downing, R. S.; Urbach, F. L. *J. Am. Chem. Soc.* **1969**, *91*, 5977.
(20) Patterson, G. S.; Holm, R. H. *Bioinorg. Chem.* **1975**, *4*, 257.
(21) Costa, G.; Mestroni, G.; Puxeddu, A.; E. Reisenhofer, E. *J. Chem. Soc. A* **1970**, 2870.
(22) (a) Gosden, G.; Healy, K. P.; Pletcher, D. *J. Chem. Soc., Dalton Trans.* **1978**, 972. (b) Higson, B. M.; McKenzie, E. D. *Inorg. Nucl. Chem. Lett.* **1970**, *6*, 209.

Table 5. Electrochemical Data for **1A**−**6A** and **1B**−**6B** in DMSO

	$\pi-\pi^*$	d−d (Cu)		$\pi-\pi^*$	d−d (Ni)	d−d (Cu)	
$CoCu(L^{2,2})$ (**1A**)	350 (7710)	540 (180)	$CuCo(L^{2,2})$ (**1B**)	369 (6720)		650 (150)	
$NiCu(L^{2,2})$ (**2A**)	355 (6180)	570 (145)	$CuNi(L^{2,2})$ (**2B**)	374 (7130)	530 (sh)	670 (95)	
$ZnCu(L^{2,2})$ (**3A**)	351 (7770)	553 (190)	$CuZn(L^{2,2})$ (**3B**)	363 (9320)		646 (120)	
$CoCu(L^{2,3})$ (**4A**)	352 (9170)	640 (106)	$CuCo(L^{2,3})$ (**4B**)	345 (9310)		571 (120)	612 (160)
$NiCu(L^{2,3})$ (**5A**)	353 (9650)	634 (110)	$CuNi(L^{2,3})$ (**5B**)	350 (9300)		587 (150)	752 (50)
$ZnCu(L^{2,3})$ (**6A**)	350 (8320)	643 (90)	$CuZn(L^{2,3})$ (**6B**)	349 (10500)		639 (120)	

Table 6. Electrochemical Data for **1A**−**6A** and **1B**−**6B**[a]

	Cu^I/Cu^{II}	M^I/M^{II}		Cu^I/Cu^{II}	M^I/M^{II}
CoCu($L^{2,2}$) (**1A**)	−1.14 (0.11)		$CuCo(L^{2,2})$ (**1B**)	−0.59 (0.06)	−1.35 (0.05)
$NiCu(L^{2,2})$ (**2A**)	−1.16 (0.11)		$CuNi(L^{2,2})$ (**2B**)	−0.48 (0.07)	−1.76 (0.06)
$ZnCu(L^{2,2})$ (**3A**)	−1.18 (0.17)		$CuZn(L^{2,2})$ (**3B**)	−0.61 (0.17)	
$CoCu(L^{2,3})$ (**4A**)	−0.92 (0.08)		$CuCo(L^{2,3})$ (**4B**)	−0.59 (0.16)	−1.64 (0.08)
$NiCu(L^{2,3})$ (**5A**)	−0.95 (0.09)	−1.76 (0.10)	$CuNi(L^{2,3})$ (**5B**)	−0.60 (0.15)	−1.56 (0.06)
$ZnCu(L^{2,3})$ (**6A**)	−0.99 (0.08)		$CuZn(L^{2,3})$ (**6B**)	−0.69 (0.12)	

[a] $(E_{pa} + E_{pc})/2$ vs Ag/Ag^+ ($\Delta E = E_{pa} - E_{pc}$). Conditions: glassy carbon working electrode, Pt auxiliary electrode, Ag/Ag^+ (TBAP/CH_3CN) reference electrode, TBAP (1×10^{-1} M) supporting electrolyte, 100 mV/s scan rate, 1×10^{-3} M complex concentration.

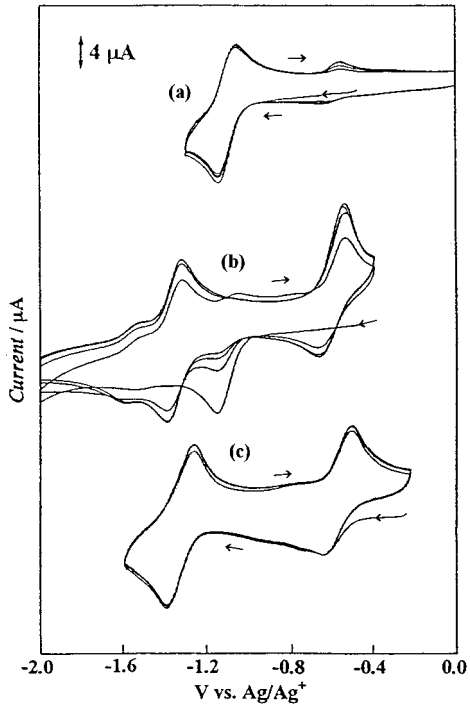

Figure 6. Cyclic voltammograms of **1A** in the sweep in the potential range of −1.3 to +0.1 V (a) and in the sweep in the range of −2.2 to −0.4 V (b). (c) is the cyclic voltammogram of **1B**.

the Co^I/Co^{II} process at the iminic site. Complex **5A** showed an additional couple at −1.76 V attributable to the Ni^I/Ni^{II} process in the aminic site. In the case of **5B** the Ni^I/Ni^{II} process in the iminic site is seen at −1.56 V.[2b]

Thus, cyclic voltammetry is proved to be an effective technique for differentiating the isomeric $M^{II}Cu^{II}$ and $Cu^{II}M^{II}$ complexes.

Isomeric Conversion in Solution. The success in preparing the isomeric $M^{II}Cu^{II}$ and $Cu^{II}M^{II}$ complexes is obviously owed to the macrocyclic effect of ligands $(L^{2,2})^{2-}$ and $(L^{2,3})^{2-}$, stabilizing the heterodinuclear core (thermodynamic effect) and retarding toward a metal dissociation in solution (kinetic effect).[23] However, the conversion of one isomeric form into another form is possible under certain conditions. Two distinct cases of such isomeric conversion are described below.

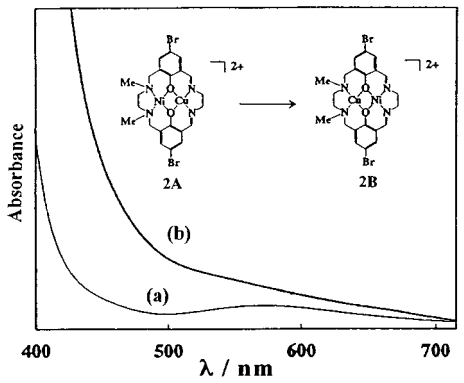

Figure 7. Visible spectral changes on heating a DMSO solution of **2A** at 70 °C: (a) just after dissolution and (b) after 12 h.

Figure 6 shows cyclic voltammograms for **1A** (CoCu) in DMSO. In the sweep down to −1.3 V, the complex showed a good stability on the electrode except for a weaker couple near −0.6 V (trace a). In the sweep down to −2.2 V, however, the couple at −1.09 decreased its intensity and was finally replaced with new two couples at −0.6 and −1.3 V (trace b). The resulting cyclic voltammogram is indeed the CV of **1B** (CuCo), demonstrating the conversion of **1A** into **1B** on the electrode. The result indicates that the $Co^{II}Cu^I$ species of $(L^{2,2})^{2-}$ is stable but the Co^ICu^I species is unstable to cause the site exchange of the metal ions.

As discussed above for **3A**, the redox wave at −1.18 V decreased with the repeat of sweep with concomitant appearance of a new couple near −0.65 V. The new redox wave is well compared to the Cu^I/Cu^{II} process of **3B** (see Table 6), implying the conversion of **3A** into **3B**. Therefore, this must be another case of isomeric conversion on an electrode.

Figure 7 shows the spectral change when a DMSO solution of **2A** (NiCu) was heated at 70 °C. A DMSO solution of **2A** assumes a green color and shows a d−d band at 570 nm (trace a). The color of the solution changes to orange after it is heated at 70 °C for 12 h and shows an absorption band around 530 nm along with a weaker band at 670 nm (trace b). The spectrum of the orange solution is exactly the same

(23) Melson, G. A. *Coordination Chemistry of Macrocyclic Compounds*; Plenum: New York, 1979.

as that of **2B**, demonstrating a thermal conversion of **2A** into **2B** in solution. It must be emphasized that **2A** is stable at ordinary temperature in DMSO at least for one week. A mechanistic study of the thermal conversion of **2A** into **2B** is under way.

In conclusion, a series of coordination-position isomeric $M^{II}Cu^{II}$ and $Cu^{II}M^{II}$ complexes are synthesized using the macrocyclic compartmental ligands $(L^{2,2})^{2-}$ and $(L^{2,3})^{2-}$. The heterodinuclear cores are stabilized kinetically and thermodynamically by the macrocyclic effect of the ligands. To the best of our knowledge, this is the first report of coordination-position isomers comprised of labile metal ions.

Acknowledgment. This work was supported by a Grant-in-Aid for Scientific Research on Priority Area "Metal-assembled Complexes" (No. 10149106) and a Grant-in-Aid for COE Research, "Design and Control of Advanced Molecular Assembly System" (No. 08CE2005), from the Ministry of Education, Science and Culture, Japan.

Supporting Information Available: Positional and thermal parameters of non-hydrogen atoms and full bond distances and angles for **1A′**, **2A′**, and **4A** in CIF format. This material is available free of charge via the Internet at http://pubs.acs.org.

IC010499D